Direct Inertial Electrostatic Confinement Propulsion at Low Power Levels

IEPC-2019-xxx

Presented at the 36th International Electric Propulsion Conference
University of Vienna • Vienna, Austria
September 15-20, 2019

Michael Winter[1], Helmut Koch, [2] and Ricky W. Green[3]
University of Kentucky, Lexington, KY 40506, USA

and

Carl R. Hartsfield[4]
Air Force Institute of Technology, WPAFB OH 45433

The performance of a cylindrical direct inertial electrostatic confinement (IEC) thruster with helical electrodes, contained in a quartz glass tube, and internal gas feeding, designed and built at the University of Kentucky (UK), is investigated with particular respect to current-voltage characteristics and generated thrust. Two thrust measurement methods are applied: At UK, a baffle plate setup was designed to measure the stagnation force generated by the IEC exhaust beam. At the Air Force Institute of Technology (AFIT), a torsion pendulum thrust stand was used. The IEC is operated with gas flows between 25 and 60 sccm of air, argon, and nitrogen. Versions of different discharge chamber length were tested with and without an endcap at UK. Thrust values below one mN are observed for the applied operating parameters.

Nomenclature

B	=	magnetic field strength, T
c_e	=	effective exhaust velocity, m/s
d	=	distance between calibration
e	=	elementary charge, 1.602 10^{-19} C
$E_{\mathrm{kin,e}}$	=	kinetic energy of electrons, eV
F	=	thrust, N
F_{cal}	=	electrostatic calibration force, N
g_0	=	acceleration on the Erath's surface, 9.81 m/s^2
I_{sp}	=	weight specific impulse, s
$\dot{m}$	=	mass flow rate, mg/s

---

[1] Assistant Professor, Department of Mechanical Engineering, Senior Research Associate at the Institute of Research for Technology Development (IR4TD), Michael.Winter@uky.edu.
[2] PhD candidate, Institute for Space Systems, University of Stuttgart, Stuttgart, Germany, helmut.koch@uky.edu.
[3] Graduate Student, Department of Mechanical Engineering, ricky.green@uky.edu.
[4] Assistant Professor Aerospace Engineering, Department of Aeronautics and Astronautics, Carl.Hartsfield@afit.edu.

M_a = mass in atomic mass units, AMU
m_e = electron mass, 9.109 10^{-31} kg
r_{beam} = bending radius of the electron beam, cm
r_{levers} = ratio of the levers to the thruster and the calibration electrodes in the thrust stand, no unit
U = voltage, V
v_e = electron velocity, km/s

I. Introduction

RECENT years have shown an increasing interest in small satellites in particular since the introduction of a standardized modular architecture in form of CubeSats in 1999 through California Polytechnic State University and Stanford University with major applications in low earth orbit (LEO). Long term missions, missions which require a particular orientation, or swarm concepts which require defined positions of individual satellites to each other demand for on-board propulsion systems. Weight and fuel restrictions call for most efficient propulsion systems, preferably with low mass flows and high specific impulses. Amongst current propulsion systems, electric propulsion is known to generate the highest specific impulses but, however, increases system complexity and comes with the penalty of additional hardware and the need of electrical power. In particular small satellites will be subject to severe power constraints given by a limited battery capacity or also limited size of solar panels. For different missions, these requirements will vary, so an ideal propulsion system should be easily scalable. For such applications, an Inertial Electrostatic Confinement (IEC) plasma creating an ion beam is proposed as a propulsion system operating at low power levels.

IEC plasma devices are a highly interesting way of generating plasmas at high temperatures and have been investigated in the past with special respect to fusion plasmas.[1-5] Fusion related applications were also investigated with respect to the development of electric propulsion systems[6,7.] Non-fusion systems involved the use of IEC devices for technical applications for surface modification and as neutron or x-ray sources.[8,9] Typical devices were operated in DC mode with moderate to high voltages at low pressures although RF IECs have been reported, too.[10]

An IEC plasma is created when a Paschen breakthrough forms between two concentric electrodes at low pressure and high voltage, and a steady discharge is formed. The electrodes consist of wire structures creating relatively homogeneous spatial electric field distributions. Ions are accelerated towards the inner cathode, penetrating the wire structure, collide with each other in the center, and create the high temperature plasma by converting their kinetic energy into thermal energy. A space charge is built up by accumulating positive ions, and a potential well confines the plasma in the center region of the inner electrode. To compensate the local space charge created and particles accumulated in this region, one or more beams form to exit the plasma cloud at a location with the lowest electric field strength.

The most common design is a configuration with two spherical electrodes. For fusion applications, the main goal is to maximize the energy density in the contained plasma, resulting in the so-called “star mode” where multiple ion beams leaving the plasma at usually random locations as shown in the first picture from the left in Fig. 1. Through modification of the electrode geometry, operational behavior can be restricted to one single ion beam which leaves the plasma at a defined location.

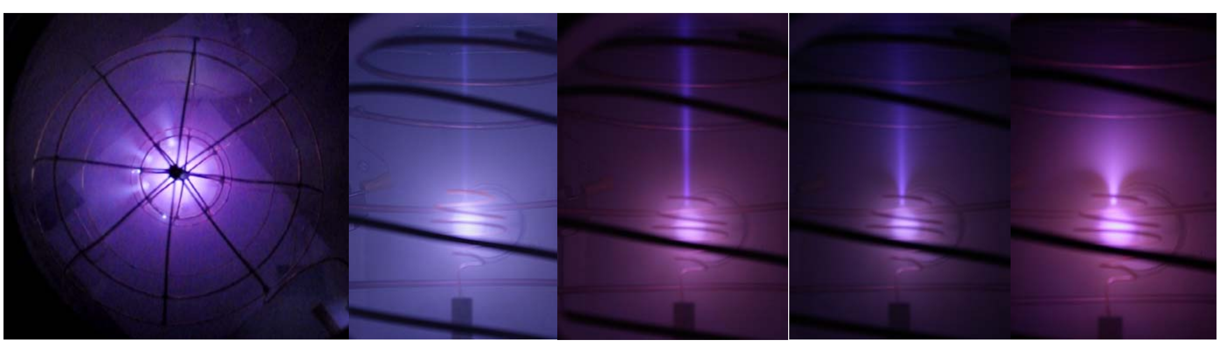

star mode 20 40 60 100 mTorr

Figure 1. IEC plasma with conventional gridded electrodes in star mode and with spherical helix electrodes in focused beam mode at different pressure levels.

Depending on power and pressure levels, this beam can be well focused or expanding (spray mode). The transition from focused beam mode to spray mode is demonstrated in Fig. 1 for increasing pressure levels with otherwise constant operating conditions. Only very recently, increased interest has been shown in using this beam for propulsion processes[11,12] and detailed knowledge about the nature of these beams is still limited.

In spray mode, a plasma beam is anticipated, recent research shows that the focused beam mainly consists of electrons leaving the IEC cavity[12]. If the focused beam is guided through a magnetic field, it indeed bends in the direction of negative charges as demonstrated at the University of Kentucky. Figure 2 shows this bent beam for a magnetic field strength of B=0.0023 T, an input power of 25 W at a voltage of 2,276 V to an open IEC in air at 25 mTorr.

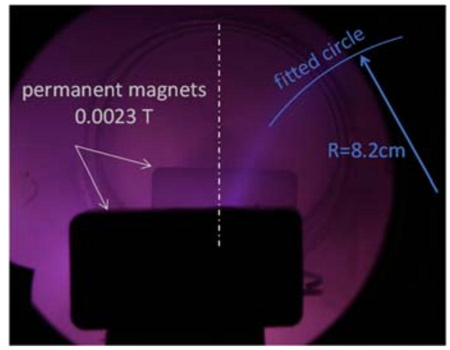

Figure 2. IEC exit beam at 25 mTorr air, 2,276 V, 25 W crossing a magnetic field of B=0.0032 T.

By equating Lorentz and centripetal forces

$$e \times v_e \times B = \frac{m_e \times v_e^2}{r_{beam}} \tag{1}$$

one obtains an equation for the velocity of the electrons

$$v_e = \frac{e \times B \times r_{beam}}{m_e} \tag{2}$$

depending on the bending radius, extracted from the image, the charge and the mass of the electron and the applied magnetic field.

For the condition shown in Fig. 2 at a power level of 25 W, a velocity of about 33,000 km/s is extracted, corresponding to an electron energy of 3.1 keV. The same experiment at 3,000 V and 56 W yields an electron velocity of 44,000 km/s equivalent to a kinetic electron energy of $E_{\text{kin,e}}$=5.5 keV.

A. IEC Development at the University of Kentucky

In the recent years, first steps have been undertaken at the University of Kentucky (UK) to develop low power IEC designs with optimized geometries with respect to robust and easy manufacturing and operational behavior.[13]

The starting point were traditional wire grid designs with first models made of copper wire with soldered joints which, however, proved not suitable due to frequent arcing preferably at the soldered joints. An initial cylindrical design was made of steel wire with point welded joints which showed rather stable operation. Finally, a geometry that does not require welding or soldering was designed by replacing the grid through a coil.

This design was very successfully tested for a range of operating conditions and was defined as the UK baseline configuration for spherical IECs. In first designs, the exit beam chose a random location until a sufficiently large gap was introduced at the pole to force the ion beam leaving the inner electrode at this location. All designs were run with residual air in the vacuum chamber at pressures between 10 mTorr and 2 Torr.

After successful operation of the spherical design, the development of a cylindrical helix configuration was started. The outer electrode was made from 2.1 mm diameter copper wire, as inner electrode, conventional steel springs were used and cut to length. For the recent versions 1 mm stainless steel wire was used to manufacture the inner electrodes due to the possibility of creating customized electrodes. These cylindrical designs qualitatively showed very similar operational behavior as the spherical ones.

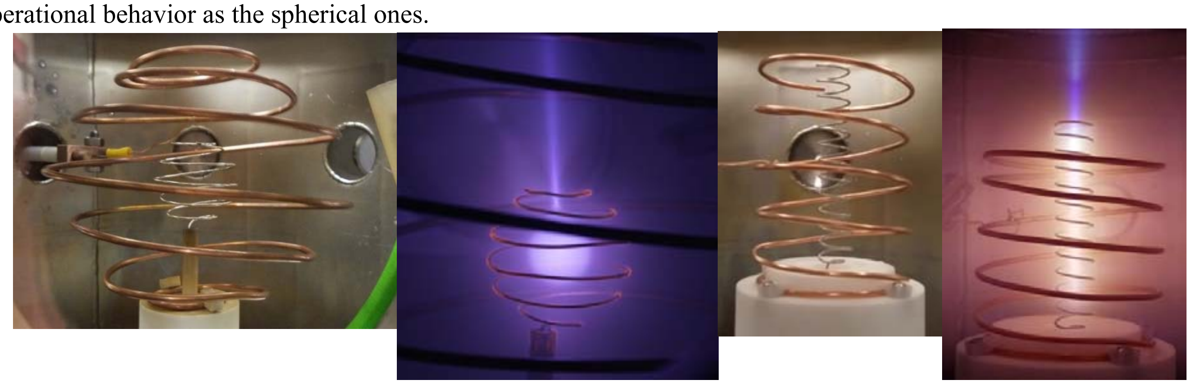

Figure 3. Spherical and cylindrical IEC helix electrode designs.

Traditional IEC systems draw the working gas from residual gas in the whole vacuum chamber. This would be interesting for in-orbit application if the rest atmosphere could be used as propellant with the benefit of not carrying propellant on-board. Unfortunately, achievable pressures and therefore particle densities in orbit seem too low to provide operating conditions sufficiently similar to those investigated so far. Most recently, an encapsulated plasma generator design was developed for the cylindrical IEC to which a defined propellant flow can be provided. This design is described in more detail in the experimental setup section.

The next step to characterize the potential of the IEC as a propulsion system was the characterization of thrust generated by the design. Unfortunately, no resources for building a suitable thrust balance were available, so a relatively simple baffle plate setup was designed and built to get first information on generated thrust levels. In addition, a first measurement campaign for directly measuring thrust on a dedicated thrust balance was conducted at the Air Force Institute of Technology (AFIT) at Wright Patterson Air Force Base in Dayton, OH. In the following, the experimental setups at the different locations are described, followed by the thruster performance at the two locations. Particular attention will be paid to describing the thrust measurements at AFIT and the reduction to thrust values.

II. Experimental Setups

The experimental setups at UK are slightly different in terms of achievable background pressure and access to the thruster. At UK, optical access to the thruster is easier but the vacuum chamber is smaller and thrust measurements can only be performed indirectly through a baffle plate setup. At AFIT, a slightly larger vacuum chamber and a thrust balance with high resolution of low thrust values are available, and lower background pressure levels can be reached. Due to the high sensitivity of the thrust balance, accessing the thruster (both optically and mechanically) is more complicated.

A. Experimental Setup at UK

The experiments were conducted in a vacuum chamber with approximately 12 inch diameter and a height of 14 inches. Vacuum was provided through a BOC Edwards XDS5 dry pump as a pre-stage and a BOC Edwards EXT255H turbo-molecular pump for vacuum levels down to about 0.1 mTorr. The pressure was controlled through a defined gas flow provided with a digital mass flow controller and measured with a Kurt Lesker 275i Pirani pressure gauge. Operation with residual air and argon at pressure levels between 10 mTorr and 2 Torr have been accomplished so far. High voltage was fed to the IEC electrodes through Lesker vacuum feed throughs with 6.35 mm diameter copper rods. Inside the chamber, the feeding cables were clamped to these rods and electrically insulated to prevent undesired discharges. The vacuum chamber has several observation ports from the side, one of which was equipped with a quartz glass window for emission spectroscopy measurements, and one flint glass window on top of the chamber. Several cameras were used to observe the IEC operation with images and video. The images presented in this paper were taken with a Nikon D610 DSLR camera controlled by a laptop computer using a CamFi remote control system.

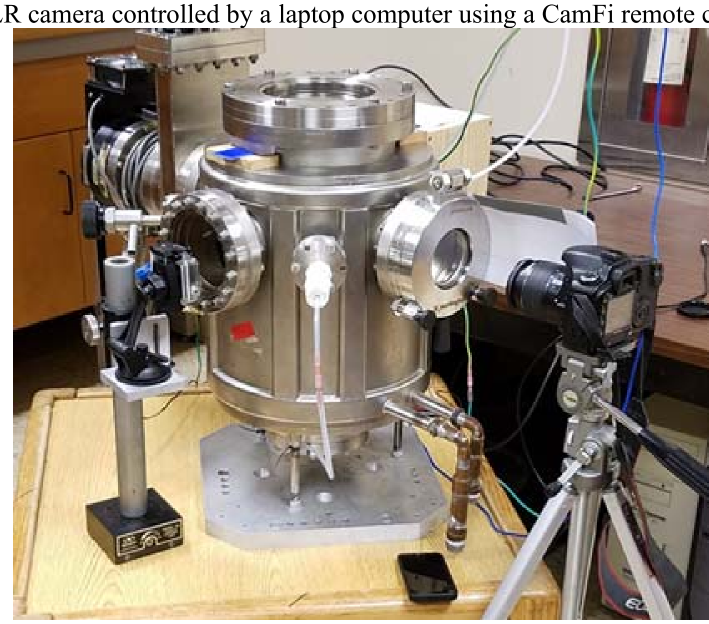

Figure 4. Vacuum chamber used for IEC plasma operation with DSLR and GoPro camera for observation.

This work focuses on cylindrical IEC designs in a quartz-glass housing with internal gas feeding (patent pending[14]) as shown in Fig. 5. The outer electrode with 1 winding every 10 mm is made of 1 mm diameter stainless steel wire, has an outer diameter of 37 mm, and is contained in a quartz glass tube of 40 mm outer diameter. The inner electrode with one winding every 2 mm is made of 0.8 mm stainless steel with an inner diameter of 7.5 mm. The working gas is supplied at the base of the plasma cavity close to the outer electrode. An additional gas feed at the center line is currently being designed to feed seed material, either for diagnostic or material sciences purposes. In a final version, the outer helix might be replaced by a metallic coating on the inside of the glass or ceramic tube which is anticipated to yield weight benefits and potentially a higher homogeneity of the electric field distribution. The design is completed by a ceramic lid which encloses the plasma cavity, thus increases the cavity pressure which is important for very low ambient pressure operation, and at the same time reduces the loss of unused working gas from the cavity.

Three different geometries mainly differing in their quartz glass tube and electrode height were chosen. The largest version provides a plasma cavity of 45 mm height, a medium and a short version with plasma cavity heights of 30 and 20 mm, respectively, were designed to avoid modes with internal discharge beam between inner and outer electrode which was occasionally observed with the longer IEC version. At AFIT, only the two shorter versions were tested.

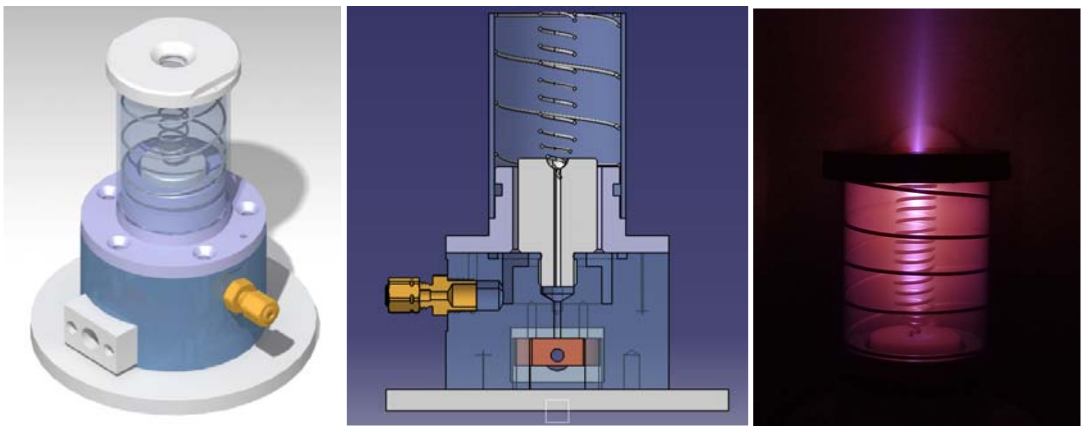

Figure 5. Confined cylindrical IEC helix electrode design with dedicated gas feed and prototype in operation with air at the UK Plasma Diagnostics Lab.

Due to missing financial resources for building a suitable thrust balance at UK, a relatively simple baffle plate setup was designed and built to get first information on created thrust levels. The IEC is installed in horizontal orientation, and a stainless steel baffle plate is hung in front of the exit plane. The location of this baffle plate can be varied between 10 and 60 mm to the IEC exit. If gas impinges on the baffle plate, a stagnation force is generated and the plate assumes a tilted position where the tilting angle is proportional to the stagnation force.

B. Experimental Setup at AFIT

Testing of the IEC took place in the Air Force Institute of Technology Geosatellite Nanopropulsion Analysis and Testing (GNAT) lab. A 0.26 m^3 chamber, built by PHPK was used. This chamber is 58 cm inside diameter, and 100 cm tall. The chamber uses an Adixen 2063-C2 roughing pump, and a Varian VHS-6 oil diffusion pump for fine pumping. Typical operating pressures are around $3.5 \cdot 10^{-5}$ Torr and can be reached in about 1-1.5 hours. It offers 36 2.75" CF flanges for placement of small optical windows, or signal and power pass-throughs, as well as a single 4" flange on the upper bell for optical access. The chamber is mounted on a table supported by Newport Optics air cushions to mitigate environmental vibration from other lab equipment. To measure thrust, a Busek torsional thrust stand[15] was used. This stand uses a Philtec Laser Displacement Sensor (DMS-D63) to measure movement of the torsion beam with a precision of 0.13 μm in the wide range mode allowing a few millimeters of motion from the torsion beam. The DMS-D63 uses the reflected power of a near-infrared laser to establish distance and can accurately measure distance from either polished, mirror-like surfaces or diffuse surfaces.[16] In this case the stand has a mirror surface at the measurement point for highest sensitivity. When coupled with the torsional springs in the flexures, this stand is capable of resolutions at the micro-Newton level. Calibration of the thrust stand is accomplished through an integrated unit delivering an electrostatic force based on voltage applied and the known distance between the two electrodes. The displacement sensor, the calibration load, and magnetic damping (both active and passive are available), are all mounted to micrometer adjusted stages to allow fine control of all three. Figure 6 shows the AFIT vacuum chamber and the IEC mounted on the Busek torsional thrust stand.

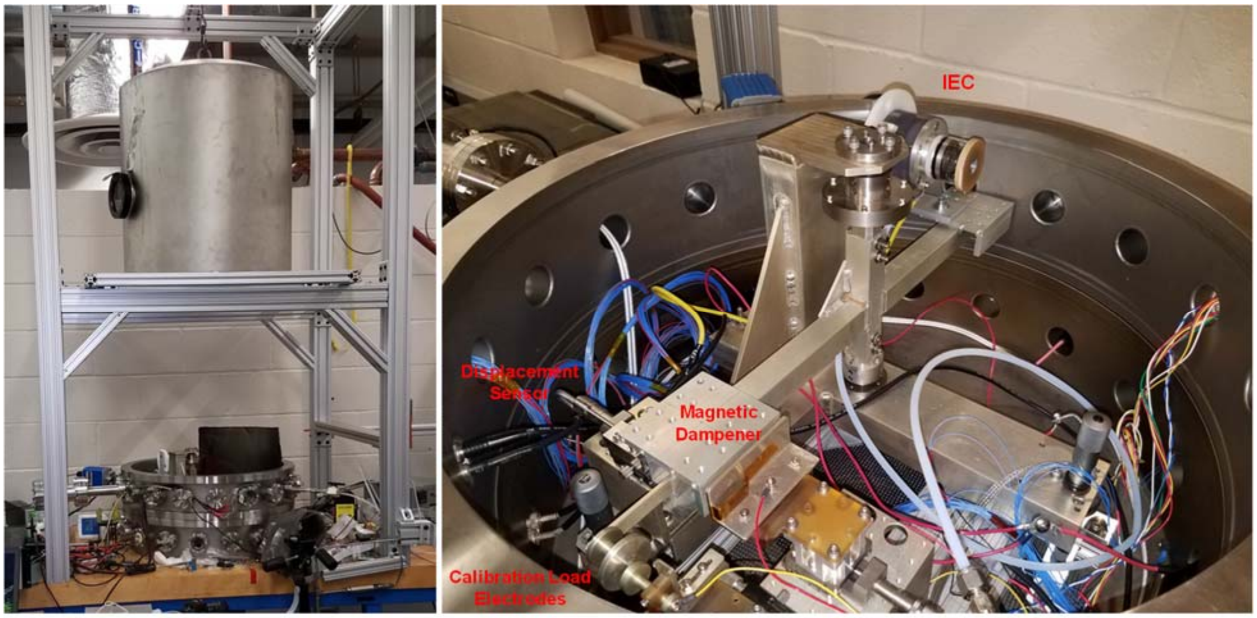

Figure 6. AFIT vacuum chamber and Busek torsional thrust stand with IEC in the chamber.

Images were captured with a Nikon D300 DSLR camera using a Sigma 105 mm lens, with autofocus compatibility and vibration reduction, mounted to a tripod outside the chamber. Opaque mats were used to block stray light and control reflections from the optical windows and the thruster was approximately 0.9 m from the camera in operation.

In operation, the power supplies, camera controls, and laser displacement sensor (LDS) readout computer were all located on a cart kept from contact with the vacuum chamber bench. This was done to minimize incidental contact and induced vibrations that could be detected by the Busek Torsional thrust stand. Even in initial setup it was noted that any contact with the bench by operators resulted in measurement output noise well in excess of the desired measurement levels. The expected thrust levels of the IEC thruster are in the neighborhood of 1 mN, leading to about 10 µm deflections in the thrust stand. Even light contact with the chamber or table resulted in 10's of µm in measured deflection, which would result in a signal to noise ratio much less than 1 during the period immediately following the contact. This excitation would damp out in a few seconds, but measurements during that period would be useless for characterization of the thruster purposes. Careful separation of the equipment researchers needed to touch from the vacuum chamber was required to accurately measure the thrust.

III. IEC Performance Data

The IEC performance is described by its mode of operation (beam or spray mode), its current-voltage characteristics and electrical mode of operation (rectified AC or DC), and by the thrust generated. Performance values such as input power, equivalent effective exhaust velocity, and equivalent specific impulse are derived from these measured values. Additional parameters are gas flow rates (air, N_2, and argon have been tested so far) and background pressure in the chamber. Due to the specific pumping systems, yielding background pressures between 1.5 and more than 100 mTorr at UK and less than 1mTorr at AFIT, the IEC operational behavior was slightly different at UK and AFIT. Due to the pumping systems, IEC operation without a lid was only possible at UK and not at AFIT. Therefore, the performance at the two locations is described in two different sections.

A. IEC performance at UK

Testing at UK involved finding operational parameters of the different IEC geometries with and without lid, operation with rectified AC and pure DC power, testing with argon, air, and N_2, and stagnation force measurements with a baffle plate setup. Although not applicable for in-space propulsion applications, the operation without a lid provides roughly the same static pressure in the discharge region as in the vacuum chamber and allows for an investigation of the influences of pressure and gas flow rate on IEC operation. The characterization with lid provides data closer to an actual propulsion system.

1. IEC performance without exit lid

During the development phase of the IEC, a rectified AC power approach was chosen at UK. A 60 Hz AC voltage, provided by a Variac source with continuously adjustable output voltage up to 120V and maximum output power of 1.4 kVA was fed into a center-tapped 9,000 V transformer with an amplification of 75 and a maximum current rating of 30 mA. The resulting output voltage was rectified through a custom-built high voltage diode circuit to maintain the electrode bias with the inner electrode being the negative pole (cathode) and the outer electrode working as the anode at ground potential. The resulting output signal oscillating with 120 Hz as illustrated in Fig. 7was supplied to the IEC. A quasi-stationary IEC plasma fluctuating with a frequency of 120 Hz was obtained for a wide variety of pressures and voltages. High speed camera imaging showed a continuously oscillating plasma beam, IEC operation was possible at voltages up to 4 kV with currents up to 30 mA.

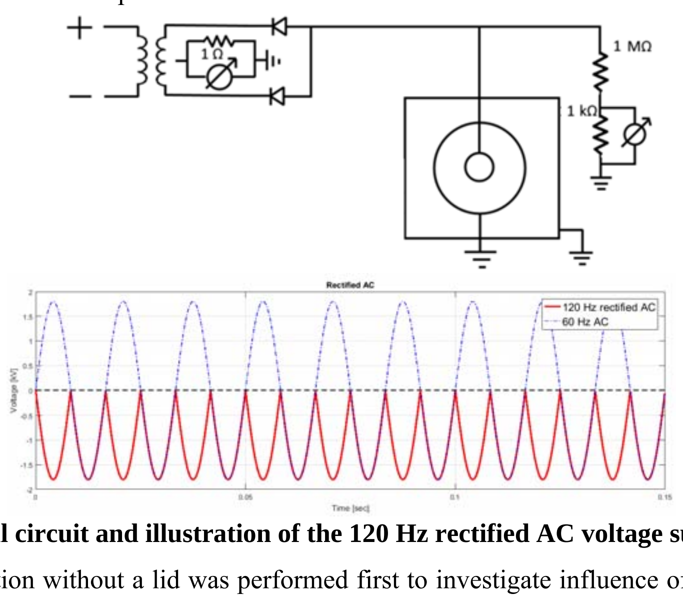

Figure 7. Electrical circuit and illustration of the 120 Hz rectified AC voltage supplied to the IEC.

Testing in a configuration without a lid was performed first to investigate influence of pressure in the discharge region and mass flow rate on the voltage-current characteristics and the operational mode of the IEC. In this configuration, the static pressure in the discharge region equals roughly the vacuum chamber pressure. From earlier experiments with a completely open configuration, it was known that beam mode operation was preferably achieved at lower pressures, and that a transition to spray mode was observed with increasing pressure.[13] To investigate the influence of mass flow rate, the vacuum chamber pressure was controlled by either fully opening the gate valve to the vacuum pump to provide highest pumping speed and controlling the chamber pressure by varying the mass flow rate applied at the base of the discharge cylinder or by applying a fixed mass flow rate and controlling the chamber pressure through partly closing the gate valve to the pump, therefore reducing the pumping speed. Figure 8 shows the current-voltage characteristic for the IEC operated in AC mode without exit lid with an air flow rate of 60.2 sccm at different chamber pressures. The gradient of current with increasing voltage increases with pressure. In this configuration, the transition to spray mode happens at a pressure of about 125 mTorr. Figure 9 shows comparisons of the IEC current-voltage characteristics for two cases where chamber pressures of 40 and 60 mTorr were achieved by applying vastly different gas flows of 40 sccm of air with a partly closed exit valve, and 129 and 154 sccm of air, respectively, at the highest pumping speed. Within the general reproducibility of these experiments, the resulting current-voltage characteristics show the same behavior. Therefore, it is concluded that the discharge characteristics are mainly controlled by the pressure in the discharge region and the mass flow rate used to maintain this pressure has only insignificant effects.

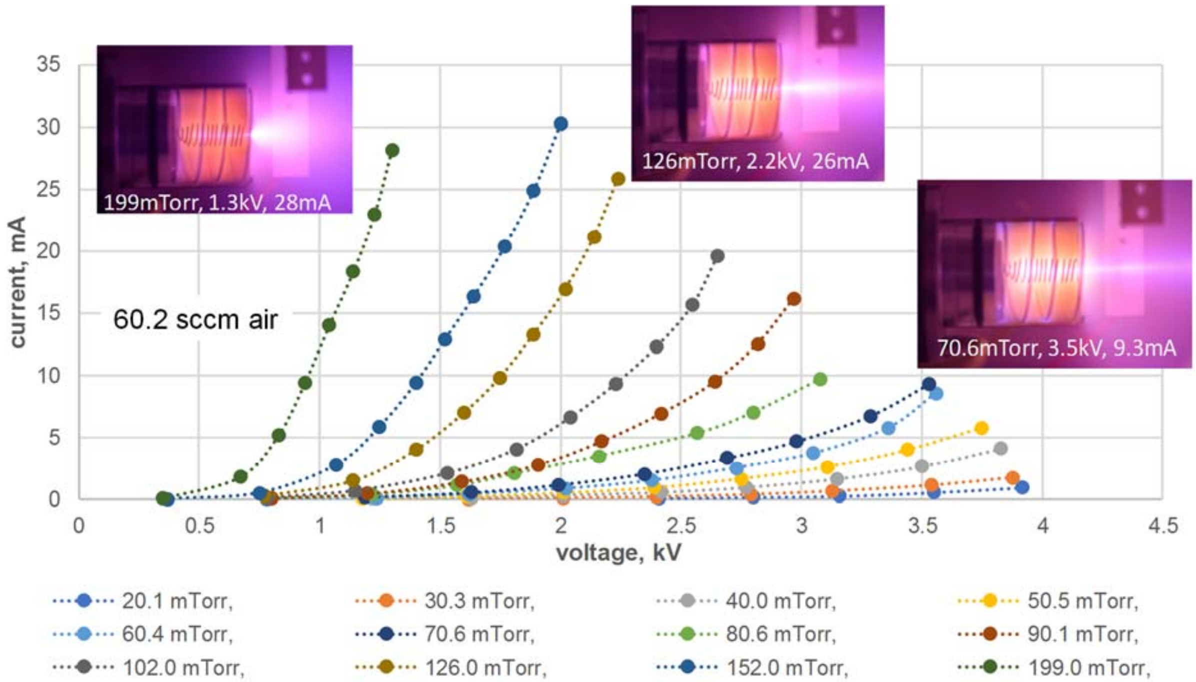

Figure 8. Current-Voltage characteristics in AC configuration with 60 sccm of air at different chamber pressures.

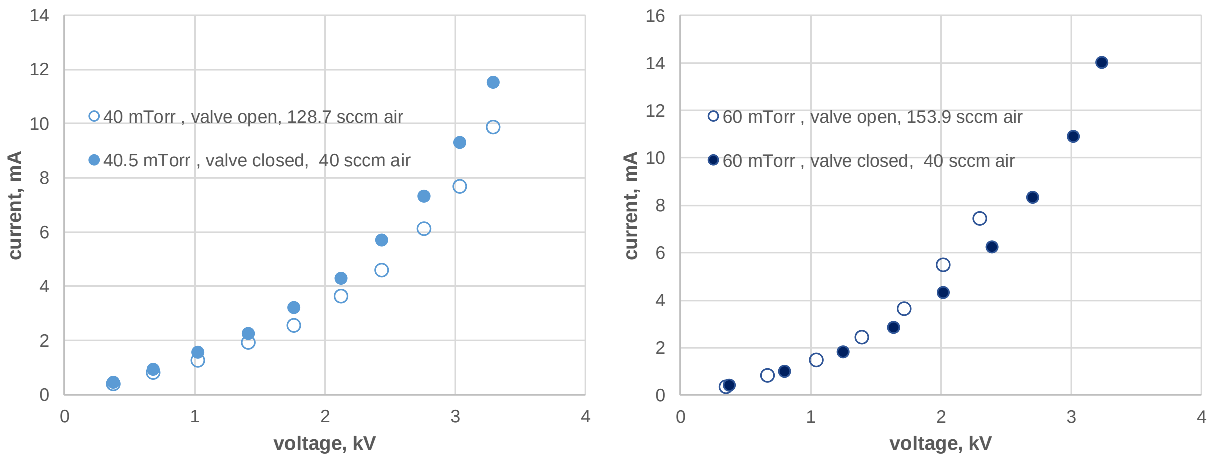

Figure 9. IEC in AC configurations at 40 and 60 mTorr chamber pressures with different gas flow rates.

Most recently, initial measurements with DC power instead of the rectified AC configuration have been conducted using a Glassman EK03R200-GW-9 Power Supply to provide current or voltage controlled power to the thruster. It is capable of delivering up to 3,000 V and 200 mA and automatically limits either current or voltage to the lower of the two control settings. This control is ideal for the IEC, taking advantage of the switch from a high voltage/low current mode to a high current/lower voltage mode as the current limit is increased, such that the voltage limit can be left at the beam mode setting.

For a limited set of gas flows of air and argon, successful operation with both electrical configurations was achieved. If operated without an exit lid, the current-voltage characteristics in rectified AC and pure DC mode are very similar as shown in Fig. 10 for a pressure of 60 mTorr at an air gas flow rate of 60.2 sccm.

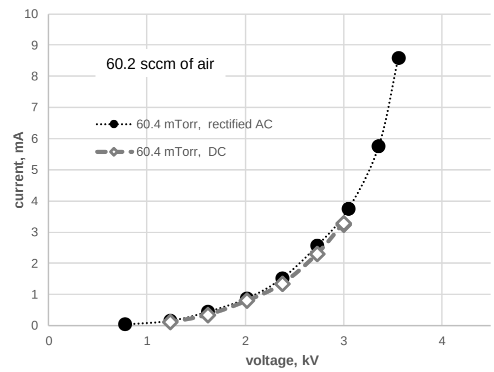

Figure 10. Comparison of current-voltage characteristics in rectified AC and DC mode.

2. IEC performance with exit lid

The final configuration as a propulsion unit is achieved by adding an end cap to the glass tube. In this configuration, ignition typically establishes in beam mode and a switch to spray mode happens. In rectified AC mode, the current-voltage characteristics are not as well behaved as in operation without an exit lid. With air, the voltage stays almost constant with increasing current, in some case even drops down if more current is provided, and drops to lower values with increasing gas flow as shown in Fig. 11a). With argon, all voltages very quickly collapse to values between 400 and 500 Vas shown in Fig. 11b).

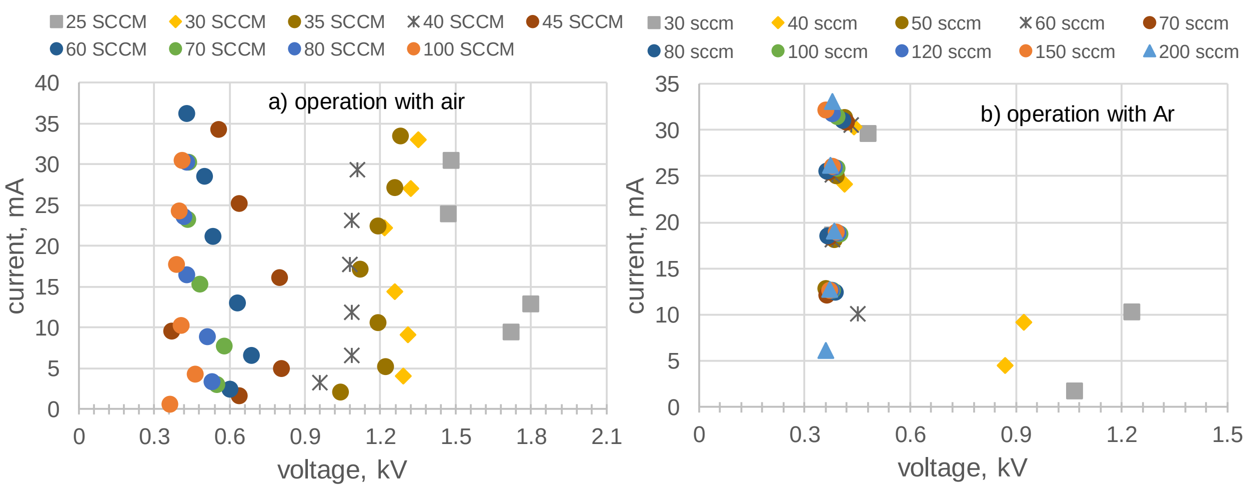

Figure 11. IEC operation with exit lid in DC configurations with air and argon.

In DC operation, a similar behavior is seen as the discharge typically ignites in beam mode and switches to spray mode, presumably as soon as a critical current is reached, if the voltage is increased sufficiently as shown in Fig. 12. With the exception of this transition regime, the current-voltage characteristics are widely linear in both discharge regimes. After switching to spray mode, the discharge is current controlled. In general, AC operation seems to enable lower currents while still providing spray mode operation. Higher achievable thrust values are anticipated in DC operation due to higher currents and steady state operation. Opposite to the anticipated behavior, the DC operation gave more defined operational conditions while rectified AC operation showed more scatter in the current-voltage characteristics as can be seen in Fig. 13.

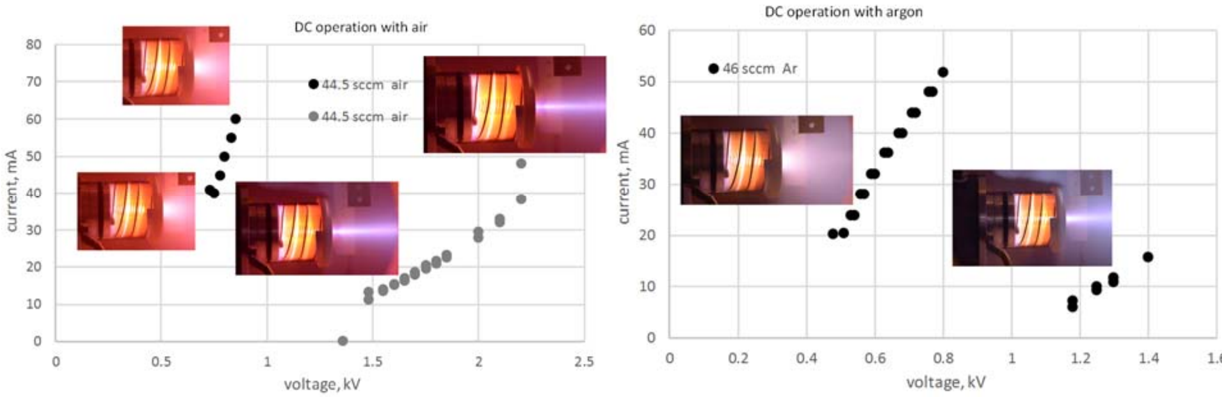

Figure 12. IEC operation with exit lid in DC configurations with air and argon.

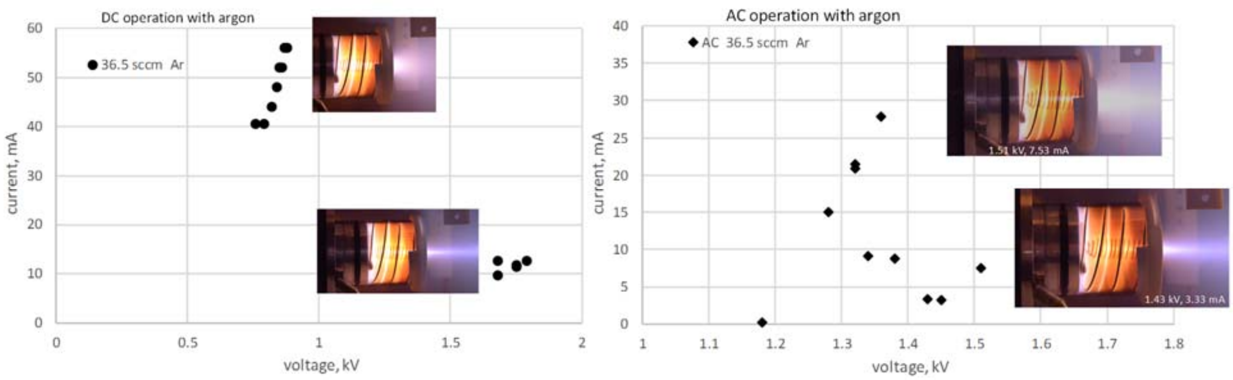

Figure 13. Comparison of IEC operation with exit lid in AC and DC configurations with argon.

3. Baffle plate measurements

For the baffle plate measurements, the IEC is installed in horizontal orientation, and a stainless steel baffle plate is hung in front of the exit plane. The location of this baffle plate can be varied between 10 and 60 mm to the IEC exit. If gas impinges on the baffle plate, a stagnation force is generated, and the plate assumes a tilted position where the tilting angle is proportional to the stagnation force. The setup as shown in Fig. 14 is mainly made of Polytetrafluoroethylene structures.

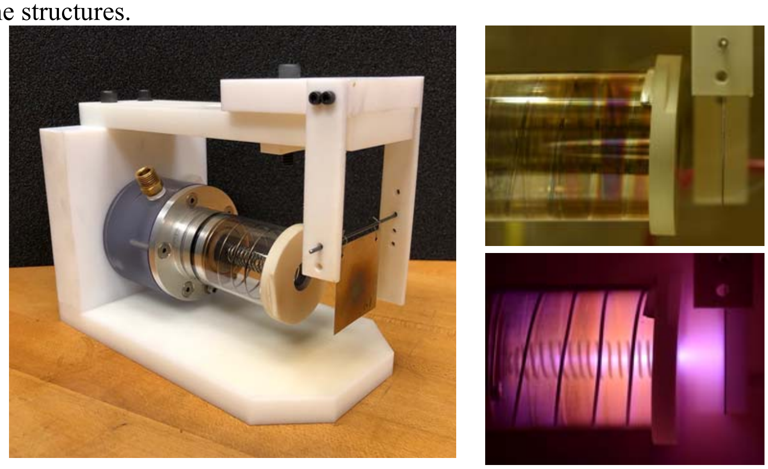

Figure 14. IEC mounted in the baffle plate setup, with and without IEC operation.

During testing, pictures of the baffle plate were taken with a commercial Nikon D610 DSLR camera and a Nikkor lens system with 105 mm focal length. Tilting angles were measured through image processing after the tests were conducted. The test procedure involved taking images without gas flow or IEC operation, images of the plate tilted through cold gas flow only, and images during IEC operation at different power levels and volume flows. Before switching to a different volume flow, the IEC power was switched off and pure cold gas and zero measurements were conducted. Air and argon were used as working gases. Although air is not an ideally suited propellant for electric propulsion, it was investigated first since an extended data base on IEC operation with the previous designs was available for comparison purposes. During this testing, a bias of the baffle plate angle, increasing with test time was noticed which was corrected for through a linear interpolation with test time.

Baffle plate measurements were conducted with air and argon. Figures 15 and 16 show the current-voltage characteristics and the cold gas forces on the baffle plate during these tests. The highest power levels of about 40 W were reached with a gas flow rate of 40 sccm of air. The higher the gas flow, the lower the maximum power levels reached.

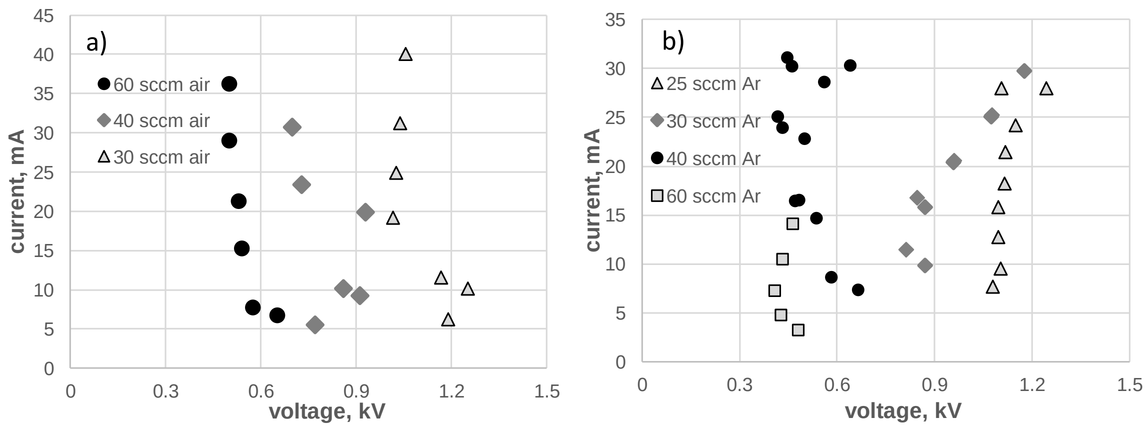

Figure 15. Current voltage characteristics of the IEC with lid in rectified AC mode during baffle plate measurements with air and argon.

The error bars in the diagrams that show baffle plate forces characterize the uncertainty in each data point introduced through the only inaccurately known distance to the pivoting point of the baffle plate. Since it was not clear whether the rotation would occur around the axis on which the wire loops holding the plate were mounted or around the connection of the baffle plate to the wires, the evaluation of the plate angle was done for both cases. The presented data points are the average of these two values, the error bars give the two extreme cases. Gas flows between 25 and 60 sccm were used, yielding cold gas forces between 0.3 and 0.7 mN, argon showing higher values than air.

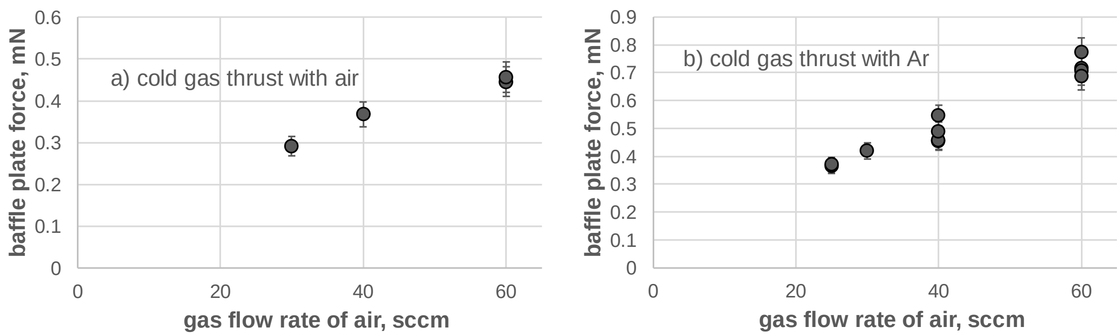

Figure 16. Measured forces on the baffle plate through cold gas with air and argon.

The baffle plate setup was indeed capable of resolving the effect of IEC operation. Figure 17 shows the measured forces on the baffle plate for different flow rates of air and argon. In each figure, the total measured force and the total force minus the cold gas force are shown to demonstrate the effect of IEC operation. With air, the IEC effect doubled the cold gas force in the best case at 30 sccm of air and an IEC power level of 32 W. For the higher gas flows, the IEC effect was clearly lower than the cold gas force, at 60 sccm of air at best 1/3 of the cold gas force was added through IEC operation. The measured forces with argon were lower than with air. Again, the lower gas flow rates yield a higher force by the IEC operation. At best, half of the cold gas force was added by IEC operation for a flow rate of 25 sccm and an IEC power of 35 W.

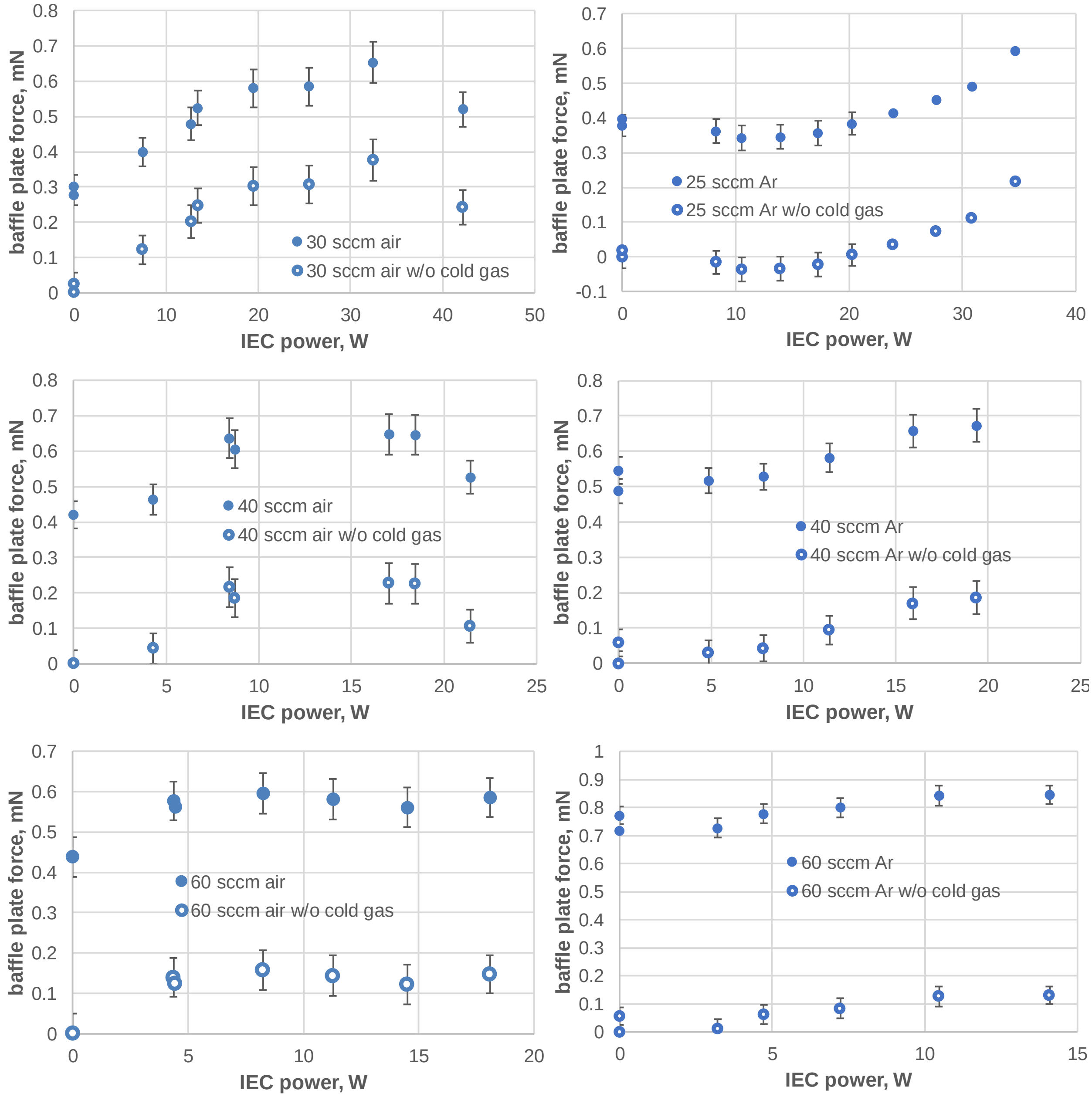

Figure 17. Measured forces on the baffle plate during IEC operation with air and argon.

Plate angles of up to 1.5 deg were seen during IEC operation with the baffle plate placed at a distance of 12 mm to the IEC exit. With volume flows between 25 and 60 sccm air or argon, and electrical input powers up to 35 W, forces on the baffle plate up to 1 mN were measured in the focused beam mode. The values with air were higher than those with argon. IEC operation resulted in about doubling the cold gas forces. So far, the best performance was seen with 30 sccm air at an electrical input power of 32 W yielding a plate force of almost 0.8 mN and an effective exhaust velocity about 1200 m/s. In spray mode, no significant force increase was measured which might be explained by high profile losses in the strongly diverging flow. These results, however, are considered highly preliminary. Within a senior design project, attempts were made to design an improved version of the baffle plate setup with reduced friction forces for the plate and an increased sensitivity by attaching a counter weight to the baffle plate. Calibration measurements were made by directing a defined air flow at the baffle plate and measuring the tilting angle. The same air flow was then directed at high sensitivity lab scales to measure a stagnation force. The results obtained with this new setup and the IEC in operation were unfortunately inconclusive and will be repeated in the near future.

B. IEC performance at AFIT

Operation was performed with argon and N2 with the short and medium length IEC configurations. With the short IEC version only spray mode operation was accomplished which, as already noticed during operation at UK with the baffle plate, did not yield detectable thrust levels. During evacuation, the thrust balance showed a significant drift, in particular after activation of the oil diffusion pumps which is attributed to a thermal effect caused by small amounts of heat from the oil diffusion pump conducted to the vacuum chamber. After some time, it reached a stable state, though. A similar drift was observed during IEC operation, again attributed to a thermal effect due to the thruster exhaust heating the chamber. Even small mechanical interaction with the chamber (e.g., touching a window flange with the cloth protecting the camera from external irradiation) caused visible ripple in the displacement signal of the thrust balance. Due to these effects, simply reading the sensor displacement was not possible. Instead, time series of the sensor output were recorded to extract the displacement data in post-processing. The final position of the displacement sensor was not necessarily predictable before evacuation. As standard operation, the sensor was set to the center of it operational range of 3 mm before evacuating the chamber. Nominally, it would return to this value after reaching steady state. The absolute value without loads applied, however, was not used for data analysis. Instead, differences between a state with and without load were extracted through linear operation as illustrated later. While operating the thruster without a lid it was observed that the thrust balance actually showed a displacement appearing as a negative thrust when voltage was applied without an ignition of the thruster. This behavior was monitored and used to correct the recorded displacement data while the thruster was operated. The following subsections describe the thrust calibration procedure, the extraction of displacement data, the voltage effect on measured displacement and the actual thrust measurements.

1. Current voltage characteristics

The corresponding values for current and voltage for each recorded data point were read from the display of the power supply and entered into a test protocol. This procedure unfortunately was not as time accurate as it would have been desirable, in particular since the thruster did actually show not as gentle operational behavior as with higher background pressures. This resulted in far more scatter and more diffuse trends than observed during the UK tests with higher background pressures, in particular for the tests with 34 and 45 sccm of argon. Also, the trend lines are shifted to lower voltages when compared to the data recorded in the UK tests.

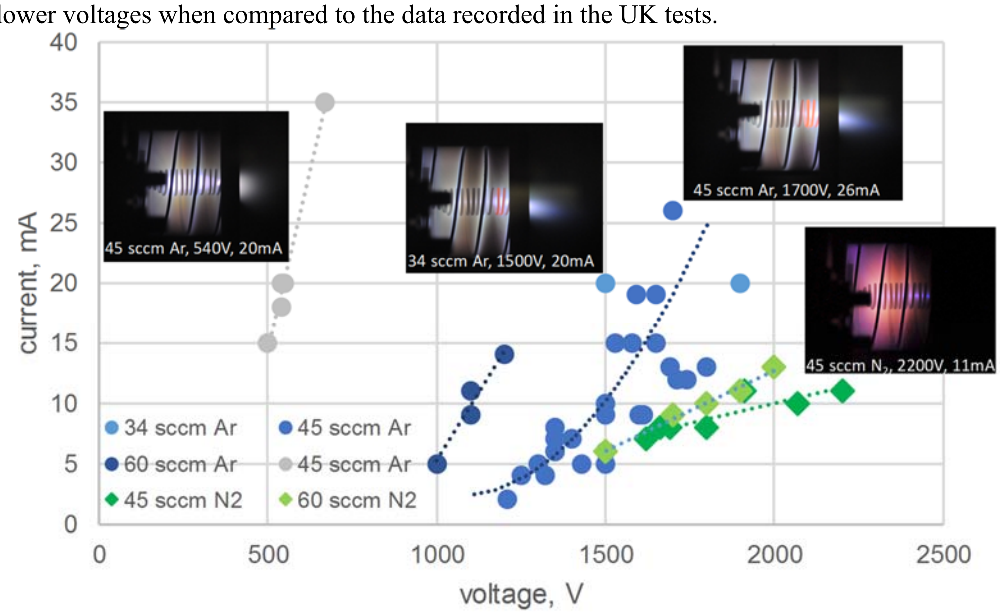

Figure 18. Current-voltage characteristics of the medium length IEC with argon and nitrogen and pictures of the IEC in operation at selected operating conditions with argon.

2. Calibration of the thrust balance

The thrust balance provides a calibration through two disk shaped electrodes which exert an electrostatic force on the balance if a voltage is applied. For a given voltage, this force depends on the distance of the electrodes to each other which can be adjusted by a micrometer stage. The calibration force F_{cal} is then calculated as:

$$F_{cal} = 1.262\ 10^{-9}\ \frac{\mu N}{V^2} \times \left(1m^2 + 138.1 \times d^2\right) \times \frac{U^2}{d^2} \tag{3}$$

with the applied voltage U in V, and the distance between the electrodes d in m. This calibration was conducted under atmospheric pressure where it was easiest to keep all parameters in useful ranges and to adjust the mechanical settings, in particular the distance between the electrodes, while taking the calibration data. An initial distance of the electrodes of 0.9 mm was chosen for the calibration which covered a maximum thrust range between 0 and 2.1 mN by applying voltages between 0 and 700 V. Still, a drift over time was noticed in the measured displacement data. Therefore, the displacement was recoded continuously while a calibration force was applied for a limited time. The drifting zero offset was interpolated by a straight line to roughly the center of the time interval the calibration force was applied and the calibration displacement was measured as the difference to that straight line as illustrated in Fig. 19. The measured displacement was used to correct the distance between the electrodes for every applied voltage. The force calculated with Eq. 3 has to be multiplied with the ratio of the levers of the electrodes and the IEC center to the axis of the torsion pendulum of r_{levers}=2.187 to yield the calibration value for the IEC thrust. The resulting calibration curve indeed is a straight line as shown in Fig. 20.

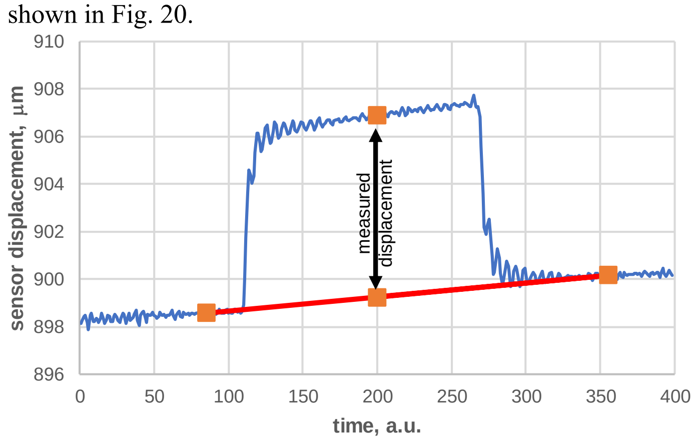

Figure 19. Illustration of the interpolation procedure for the sensor displacement during calibration.

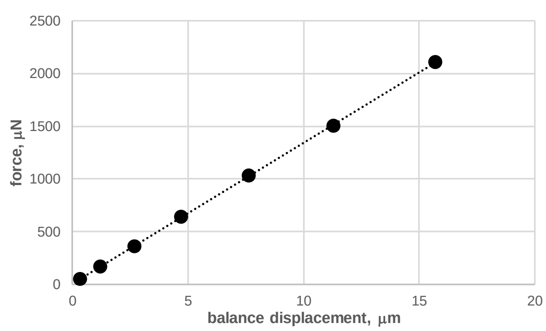

Figure 20. Thrust calibration function.

3. Effect of applied voltage

During a nitrogen test without lid, displacement of the sensor with applied voltage was observed although no thruster operation was accomplished. The displacement caused an apparent negative thrust which needed to be accounted for. In a dedicated test without gas flow, voltages up to 3 kV were applied. Additional data points were recorded for various gas flows by dialing in a voltage without allowing for a current. No significant influence of gas flow rate can be seen. The ensemble of all available data points was fitted by a second order polynomial function as shown in Fig. 21, to be used for correcting actual thrust measurements. A second order polynomial was chosen instead of a potentially better fitting straight line since physics dictate that the influence of voltage has to approach zero if no voltage is applied. The scatter of the available data indicates that the chosen correction function is indeed anticipated to introduce some additional error to the thrust data, but the correction is actually on the order of measured thrust values and therefore needed to correct the subsequent data.

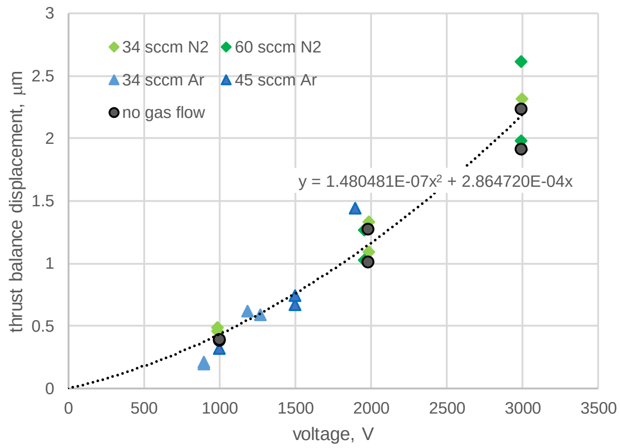

Figure 21. Effect of applied voltage for various gas flow rates of argon and N_2.

4. Cold gas thrust

At various times during each measurement series, the gas flow was switched on and off to gather data on the cold gas thrust as shown in Fig. 22. To determine the corresponding displacement value from the measured data, two straight lines were fit left and right of the observed jump similar to the procedure of thrust calibration and interpolated to the jump position. The cold gas thrust shows an approximately linear behavior. However, the values determined from the jump for switching the gas flow off are typically higher by about 10% than the corresponding value for switching on the gas flow. A reason for this behavior is still to be found. For determination of the thrust values in the next section, the average value of all available data points for each corresponding gas flow was added to the incremental values for each thruster condition. The value of about 300 mN for 45 sccm of argon was considered an outlier and ignored.

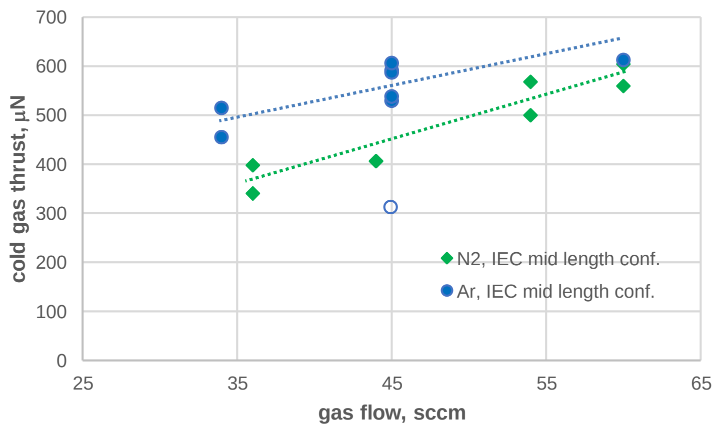

Figure 22. Cold gas thrust for various gas flow rates of argon and N_2.

5. Thrust values in operation with argon

During the first measurement campaign, no valid thrust measurements with nitrogen could be achieved. Measurements with the short IEC version, which only worked in spray mode and did not show beam mode behavior at all, did not lead to clear thrust values, although these measurements happened in the first tests with thruster operation. Future tests with refined data acquisition methods and strategies based on the recent measurements might actually yield valid thrust data.

Detectable thrust values were achieved with the medium length IEC in beam mode for gas flows of 34 and 45 sccm of argon. Due to the low background pressure, the electron beam was not as clearly visible as with the higher background pressures during the UK measurements, but the operational mode was clearly visible in the current-voltage characteristics. At multiple times, a spontaneous transition from beam to spray mode was observed in both the visual appearance of the beam and in a sudden drop in voltage from clearly beyond 1000 V to values between 500 and 650 V. This transition was usually accompanied by a drop in displacement or thrust. The thrust values reported here were determined from the usually drifting displacement data by fitting straight lines left and right of the event of concern and extrapolated to the jump position, as already mentioned for the cold gas measurements. This incremental value was the corrected by the voltage induced offset from the fitting curve shown in Fig. 21 and converted to thrust values by the calibration function from Fig. 20 to which the corresponding cold gas thrust was added. Figure 23 shows the resulting thrust values with the cold gas thrust added as straight lines. Values for 45 sccm were obtained in two separate tests, the results show some offset between the two test series. In general, the cold gas thrust is raised by 20 to 80% at power levels between 10 and 38 W, respectively.

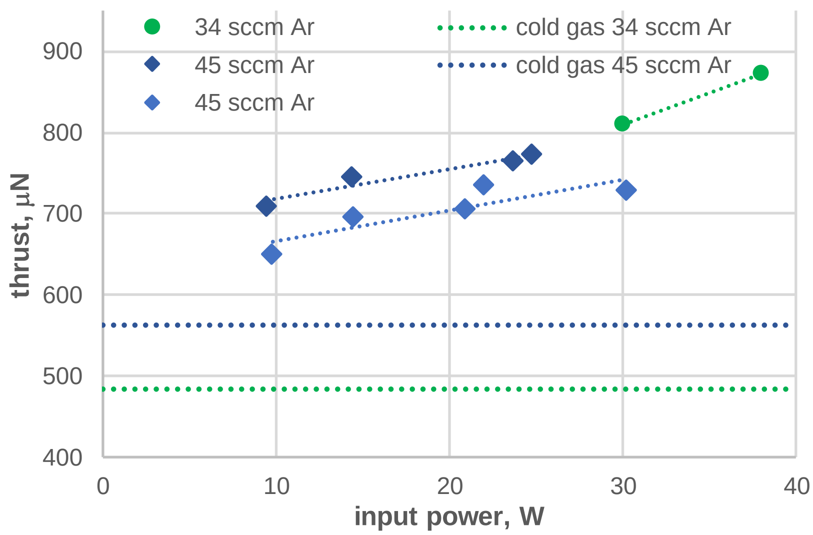

Figure 23. Measured IEC thrust for gas flow rates of 34 and 45 sccm of argon.

IV. Discussion of the Results

To characterize the performance of an electric propulsion system, usually the effective exhaust velocity c_e and the weight specific impulse I_{sp} are widely used. However, the beam mode mainly consists of an electron beam (at least as far as thrust is concerned), with electron velocities on the order of ten thousands of km/s (compare Section I). Therefore, the formulation of an effective exhaust velocity or a specific impulse makes physically only limited sense since it refers to the heavy particle gas flow (which apparently are not significantly accelerated). However, since c_e and I_{sp} are well established quantities to characterize electric propulsion in general, equivalent values have been calculated to provide a comparison with other systems. The effective exhaust velocity is related to the generated thrust through the mass flow of the operating gas:

$$F = c_e \times \dot{m} \tag{4}$$

The mass flow can be calculated from the volume flow by[17]:

$$1 sccm = 7.43583\ 10^{-4} \times M_a \left[\frac{mg}{s}\right] \tag{5}$$

where M_a is the propellant mass in atomic mass units (AMU). M_a=39.948 AMU was used to convert the volumetric gas flows used to mass flow to calculate c_e from Eq. 4. The specific impulse is obtained by dividing c_e by the gravitational acceleration on the Erath's surface g_0. For the highest thrust values, a specific impulse of 91 s can be calculated. This is significantly above the maximum achievable cold gas values for argon but seems not yet attractive for going through the effort of installing an electric propulsion system. However, it has been shown in UK testing that the mass flow is actually not the defining quantity for the IEC operation. Instead, the discharge characteristics are governed by the pressure in the discharge chamber. Currently, the exit cross section of the lid has a diameter of 10.9 mm, slightly larger than the outer diameter of the inner electrode of 9.1 mm, but significantly larger than the diameter of the electron beam which is on the order of 2 mm. As a first order approach, a lower mass flow would be required to maintain the pressure inside the IEC if the exit cross section were smaller. If the beam characteristics (dominating the thrust values) can be maintained when reducing the exit cross section diameter to one third of its current value, the necessary mass flow for maintaining the current pressure values inside the IEC would decrease by roughly a factor of 10. If the IEC thrust levels would remain the same (which is anticipated, at least roughly) the total thrust would decrease by the reduction in cold gas thrust but maximum specific impulse values of about 450 s would be reached which would make the IEC a valuable alternative for nano propulsion systems. Future modifications of the current IEC design will explore this design approach.

V. Conclusions

A cylindrical IEC model with helical electrodes, contained in a quartz glass tube, and internal gas feeding was designed and built at the University of Kentucky. Versions of different discharge chamber length were tested with and without an endcap with argon and air as operating gases at UK. A baffle plate setup to obtain first thrust estimates was designed and tested at UK. Thrust measurements on a torsion thrust balance were conducted at the Air Force Institute of Technology at Wright Patterson Air Force Base in Dayton, OH with argon and nitrogen as propellants.

The results from the direct thrust measurements at AFIT confirmed the order of magnitude of the baffle plate measurements at UK. However, differences in thrust values and operational behavior were observed which are associated to the different background pressures during operation. Measured thrust values are on the order of one mN and below in focused beam mode associated to the electron beam leaving the IEC. In spray mode, significantly lower thrust values are observed. Up to half of that thrust can be assigned to the IEC operation on top of the cold gas flow. For argon, these thrust values correspond to equivalent specific impulses slightly less than 100 s. However, the discharge characteristics were demonstrated to depend mainly on the pressure in the discharge chamber and not on the gas flow rate provided. A smaller exit cross section would still allow the electron beam to leave the discharge region but would require significantly lower gas flows to maintain the discharge region pressures necessary for IEC operation. Projected specific impulses for an exit cross section reduced to one third of the current value are on the order of 500 s, if the electron beam properties are maintained. Corresponding experiments are in preparation.

For future experiments, a transition from hand-manufactured electrodes, which lack in reproducibility, to machined electrodes with less geometry variations is intended to reduce variability of the results obtained with different electrodes. Furthermore, the stainless steel electrodes (in particular the inner electrode) showed significant ablation during extended operation, covering the inside of the glass tube with a thin ablation layer. A transition to a high temperature resistant electrode material such as tungsten, potentially through 3D printing, is intended. A modified version with a secondary axial gas feed has been designed to provide the ability of seeding the plasma with tracer materials for coating or diagnostic purposes. In future experiments, this secondary gas feed line can also be used for directly measuring the pressure in the discharge region to better control the discharge mode.

Acknowledgments

The authors would like to acknowledge three University of Kentucky senior design teams in the period from Fall 2015 to Spring 2019, namely Connor Johnstone, Troy Soileau, Kody Grilz, Josh Little, Ken Freeman, Brett Emerson, Jacob Catchen, Lucas Morrison, Rob Hughes, Matt Wetherell, and Tristan Hagerman for their engaged and inventive contributions, as well as the Department of Mechanical Engineering for supporting these three projects. Furthermore, the authors would like to thank Georg Herdrich (University of Stuttgart), Richard Anderson and Todd Hastings (EE Department University of Kentucky), as well as Bill Fuqua for important and helpful advice, and Bradley Butler, Julian Beyer, Avery Hartley, and Tawn Dang for help with setup, preliminary data acquisition and analysis, and Floyd

Taylor at UK for help with manufacturing. The authors also thank the AFIT Department of Aeronautics and Astronautics laboratory staff, and the AFIT Research & Sponsored Programs staff.

References

[1] Messier, Douglas (22 May 2015). "Tiny 'Cubesats' Gaining Bigger Role in Space". Space.com. Retrieved 2015-05-23.

[2] Helvajian, Henry; Janson, Siegfried W., eds. (2008). Small Satellites: Past, Present, and Future. El Segundo, Calif.: Aerospace Press. ISBN 978-1-884989-22-3.

[3] Hirsch, R.L.; Apparatus for generating fusion reactions, Patent US3530036.

[4] R.L. Hirsch, "Inertial-electrostatic confinement of ionized fusion gases", Journal of Applied Physics 38, 4522-4534 (1967).

[5] G. R. Piefer, John F. Santarius, Robert P. Ashley, Gerald L. Kulcinski, "Design of an Ion Source for 3He Fusion in a Low Pressure IEC Device," Fusion Science and Technology 47, 1255-1259 (2005).

[6] G.H. Miley et al., "Inertial Electrostatic Confinement as a Power Source for Electric Propulsion," Proceedings of the NASA Vision-21 Conference, NASA Lewis Research Center, Cleveland, OH, 30-31 March 1993.

[7] R.W. Bussard and L.W. Jameson, "Inertial-Electrostatic-Fusion Propulsion Spectrum: Air-Breathing to Interstellar Flight," Journal of Propulsion and Power, 11:365-372, March-April 1995.

[8] G. H. Miley, L. Wu, H. J. Kim, "IEC-based neutron generator for security inspection system", Journal of Radioanalytical and Nuclear Chemistry 263, 1, 159-164 (2005).

[9] Y. Gu and G.H. Miley, "Spherical IEC Device as a Tunable X-Ray Source," Bulletin of the American Physical Society: 40:1851, 1995.

[10] S. KrupakarMurali Æ John F. Santarius Æ Gerald L. Kulcinski, "Study of Various Modes of Operation of an IEC Device," Fusion Energy (2010) 29:141–145, DOI 10.1007/s10894-009-9246-6.

[11] Herdrich, G., Syring, C., Torgau, T., Chan, Y. A., and Petkow, D., "An Approach for Thrust and Losses in Inertial Electrostatic Confinement Devices for Electric Propulsion Applications," 34th International Electric Propulsion Conference, Kobe, Japan, 2015.

[12] Yung-An Chan and Georg Herdrich, "Inertial Electrostatic Confinement: Innovation for Electric Propulsion and Plasma Systems," proceedings of The 35th International Electric Propulsion Conference, Georgia Institute of Technology, USA, October 8 – 12, 2017.

[13] Winter, M., Koch, H., "Inertial Electrostatic Confinement Plasma Devices – Potential thruster technology for very accurate attitude control systems," 35th International Electric Propulsion Conference (IEPC), October 8 – 12, 2017, Atlanta, Georgia.

[14] Michael Winter, Helmut Koch, Inertial Electrostatic Confinement (IEC) plasma generator module with defined gas feeding, U.S. Provisional Patent App. Ser. No. 62/744,377, filed on October 11, 2018.

[15] Torsional Balance System Operating Manual, Busek Co., Inc, October 2007, Natick MA 01760-1023, 11 Tech Circle.

[16] PhilTec, Inc. August 2019, Model D63 Reflectance Dependent Analog Sensor Data Sheet., https://philtec.com/downloadssupport/documentlibrary/documents/datasheets/analog%20only/D63.pdf.

[17] Dan M. Goebel and Ira Katz," Fundamentals of Electric Propulsion: Ion and Hall Thrusters," John Wiley & Sons, Inc., July 2008, print ISBN:9780470429273, |online ISBN:9780470436448, DOI:10.1002/9780470436448.